Unsteady Flows and Airfoil-Vortex Interaction

M. Mamou, M. Khalid and H. Xu
Institute for Aerospace Research
National Research Council
Ottawa, K1A 0R6, Ontario, Canada
Mahmoud.Mamou@nrc.ca

Abstract

Unsteady flows past two airfoils in tandem placed in a shock tube flowfield have been studied using Navier-Stokes equations. An implicit Global Newton iterative procedure is applied for time accurate solution of the transient flowfield. This study is primarily motivated by a need to understand the aerodynamic implications of the blade-vortex interaction in the rotor flowfield of a helicopter. To simulate the vortex effects in 2D, a streamwise moving shock wave is imposed immediately upstream of the leading edge of the lead airfoil, which is pitched at an angle of attack of –20 degrees. The lead airfoil is used to generate a vortex that can be lifted off and convected downstream until it reaches the trailing test airfoil. After the passage of the shock wave over the lead airfoil, a nearly symmetric vortex is generated. This vortex, then, separates at the trailing edge and convects downstream at the freestream velocity towards the aft airfoil. To avoid numerical dissipation, a refined grid is used along the vortex path. For the aft airfoil, it is observed that the passage of the vortex has notable affects upon its aerodynamic characteristics. It is further noted that the vortex is followed by the lead airfoil wake, which splits later on into series of smaller vortices. Owing to the high angle of attack of the lead airfoil, the viscous flow underneath seems to progressively grow behind the shock wave resulting in a separation. The flowfield is seen to comprise of a complex pattern of incident and reflected compressibility waves from the walls, which interact with the separated flow presents on the lower airfoil surface.

Introduction

Understanding vortical flows is important in most areas of fluid dynamics. Once evolved, the presence of vortices affects the resulting aerodynamic performance. The leading edge vortices from the wings of a fighter aircraft under certain attitude and flow conditions could reduce the performance dramatically. The tip vortices from a large passenger aircraft in ascent mode can persist for many minutes, effectively preventing the usage of runway by smaller aircraft. The winglets are sometimes used to reduce the strength of the wing tip vortex system and the induced drag. Very often vortex generators are installed on the wing surfaces of commercial airliners to augment lift performance. For simulating the flows on propeller-powered vehicles and other rotorcraft flowfield, the designers have wrestled with blade-vortex interaction (BVI) problems for decades. The flow simulation, in this case, does not only have to contend with the tracking of the three-dimensional rotor wake, which is continuously updated in real time with intermittent flow separation effects, but also has to accommodate the evolution and the dissipation of the tip vortices in the flowfield. At any given time, the vortices shed from the leading blades interact with and impinge upon the trailing blades, giving rise to a host of noise and vibration issues [1]. These problems become even more challenging when one considers the variety of flight conditions under which a helicopter is expected to function.

Paper presented at the RTO AVT Symposium on "Advanced Flow Management: Part A – Vortex Flows and High Angle of Attack for Military Vehicles", held in Loen, Norway, 7-11 May 2001, and published in RTO-MP-069(I).

Report Documentation Page

Form Approved
OMB No. 0704-0188

Public reporting burden for the collection of information is estimated to average 1 hour per response, including the time for reviewing instructions, searching existing data sources, gathering and maintaining the data needed, and completing and reviewing the collection of information. Send comments regarding this burden estimate or any other aspect of this collection of information, including suggestions for reducing this burden, to Washington Headquarters Services, Directorate for Information Operations and Reports, 1215 Jefferson Davis Highway, Suite 1204, Arlington VA 22202-4302. Respondents should be aware that notwithstanding any other provision of law, no person shall be subject to a penalty for failing to comply with a collection of information if it does not display a currently valid OMB control number.

1. REPORT DATE	2. REPORT TYPE	3. DATES COVERED
00 MAR 2003	**N/A**	**-**

4. TITLE AND SUBTITLE	5a. CONTRACT NUMBER
Unsteady Flows and Airfoil-Vortex Interaction	5b. GRANT NUMBER
	5c. PROGRAM ELEMENT NUMBER
6. AUTHOR(S)	5d. PROJECT NUMBER
	5e. TASK NUMBER
	5f. WORK UNIT NUMBER
7. PERFORMING ORGANIZATION NAME(S) AND ADDRESS(ES) **NATO Research and Technology OrganisationBP 25, 7 Rue Ancelle, F-92201 Neuilly-Sue-Seine Cedex, France**	8. PERFORMING ORGANIZATION REPORT NUMBER
9. SPONSORING/MONITORING AGENCY NAME(S) AND ADDRESS(ES)	10. SPONSOR/MONITOR'S ACRONYM(S)
	11. SPONSOR/MONITOR'S REPORT NUMBER(S)

12. DISTRIBUTION/AVAILABILITY STATEMENT
Approved for public release, distribution unlimited

13. SUPPLEMENTARY NOTES
Also see: ADM001490, Presented at RTO Applied Vehicle Technology Panel (AVT) Symposium held inLeon, Norway on 7-11 May 2001, The original document contains color images.

14. ABSTRACT

15. SUBJECT TERMS

16. SECURITY CLASSIFICATION OF:			17. LIMITATION OF ABSTRACT	18. NUMBER OF PAGES	19a. NAME OF RESPONSIBLE PERSON
a. REPORT	b. ABSTRACT	c. THIS PAGE			
unclassified	**unclassified**	**unclassified**	**UU**	**14**	

Dealing with the physics of the problem is one issue: coming up with the computational resources for adequate modeling in real time is quite another. A three-dimensional modeling of a complete rotor-on helicopter in an unsteady flowfield would require prohibitive computational resources. The present work deals with the two-dimensional modeling of the flow between two airfoils, effectively representing the time dependent flow past the cross section of two rotor blades.

In an attempt to accurately model the aerodynamic flowfield between two airfoils along the line of the rotor blade flow, an unsteady viscous computation is conducted on a high density packed grid. Accurate blade wake prediction using Navier-Stokes equations are rendered inaccurate due to the numerical dissipation and truncation errors to produce faster averaged solutions. For airfoil vortex interaction (AVI) studies, a majority of previous theoretical studies were carried out by supplanting (mathematically) a vortex seed upon a freestream flow in close vicinity of the leading edge of an airfoil. The vortex is then in turn convected downstream where it interacts with the airfoil structure [1, 2, 3 and 4]. In such studies, the vortical flow generation is based on the experimental observation.

In a conventional two-chamber shock tube, acoustic waves, resulting from parallel AVI, were studied experimentally by Kaminski and Szumowski [5]. It was observed that the vortex, which is generated by a lead airfoil, breaks-up as it encounters the leading edge of the aft airfoil and produces induced oscillatory flows. As a result, acoustic waves are generated during the AVI process. Later on, for the same type of experiment, Selerowicz et al. [6], studied the effect of the miss-distance (distance between the vortex core and a horizontal line passing through the leading edge of the aft airfoil) in terms of the AVI phenomenon. It was observed that when the vortex impinges or passes close to the airfoil, the aerodynamic loads are considerably affected. Using Euler-based CFD on the unstructured grids, Piechna and Szumowski [2], as well as Sobieraj et al. [3], carried out numerical modeling of the typical AVI behavior. Their numerical domain, however, was limited to the test airfoil region and a simplified model study was carried out by seeding a pre-defined vortex upstream of an airfoil and by computing the complete unsteady flowfield as the vortex traversed past the airfoil. Using sufficiently high grid density, they found that the flow behavior, when the vortex passes over the airfoil, agrees qualitatively well with the experimental observation [3].

The above research concerns only a parallel AVI. For perpendicular BVI, Wittmer and Devenport [7,8] studied this phenomenon experimentally by considering two NACA 0012 blades in tandem. The leading blade was used to generate the tip vortex that interacts with the aft blade. Their measurement indicates that, when the vortex passes over the blade, the flow turbulence in the blade wake triggers the turbulence decay of the vortex core. As a result, the vortex increases in size and loses its strength and circulation. It was also found that the effects of the interaction are slightly affected by the angle of attack of the blade and the vortex strength.

The issue of excessive numerical dissipation in wing-tip vortex flows was also recently addressed by Spall [9] using Euler equations and second-order accurate pressure-based finite volume algorithm. The mesh was built with a higher grid density along the vortex core path. The comparison of the computed results against available experimental data showed that the vortex strength and its core size are well preserved down to 10 chords from the leading edge of the wing. This particular approach is regarded as a viable alternative to the high-order numerical scheme resolution.

In the present paper, following the numerical study of Spall [9], the AVI is studied numerically using a Navier-Stokes equations based simulation. The geometry configuration described in [3] is adapted for the current model. In the previous studies, AVI problem is conducted by superposing mathematically a vortex to a freestream just near the leading edge of the airfoil. In the present study, however, two NACA 0012 airfoils in tandem are considered for the AVI process. The first

airfoil (lead airfoil), placed upstream at a given angle of attack, is used to generate a vortex. The second airfoil (aft airfoil), located 5.4 chords downstream, is regarded as a test airfoil which will interact with the vortex germinated by the lead airfoil. The results show that the present approach is capable of not only predicting the generation and traverse of a vortex, but also simulate the AVI process. The results are seen to agree qualitatively well with the experimental results [3].

Geometry Description

The experimental facility and apparatus described in Ref. [3] is duly adapted for the current investigation. The apparatus consists of a rectangular shock tube in which two NACA 0012 airfoils are mounted in tandem. The cross-section of the test area is shown in Figure 1. The lead airfoil is regarded as a vortex generator. The angle of attack could be adjusted by rotating the airfoil about an axis situated at 0.25c from the leading edge. The aft airfoil is used for AVI process. The angle of attack for the aft airfoil is maintained at 5 degrees, nose up. The miss-distance could be controlled by the vertical movement of the lead airfoil (distance between the vortex core and the horizontal line passing through the leading edge of the aft airfoil). As described in the experiment [3], after the diaphragm breaks, the freestream behind the shock wave could be assumed steady for a period of time of 1.6 to 9.1 ms. The freestream conditions are given by M_∞=0.69 and p_∞=3.278 psi. As displayed in Figure 1, when the shock wave passes over the lead airfoil, a vortex is formed at the trailing edge of the lead airfoil. After detachment from the mother airfoil, the vortex is convected downstream and is in turn intercepted by the aft airfoil. The AVI process effectively involves the ensuing flowfield response in between the vortex and the aft airfoil. The distance between the two airfoils is taken to be 5.4c (where c is the airfoil chord length of 120 mm), which is sufficient enough for shock wave recovery, when passed over the lead airfoil. It is observed that the shock wave, when leaving the trailing edge, is severely distorted.

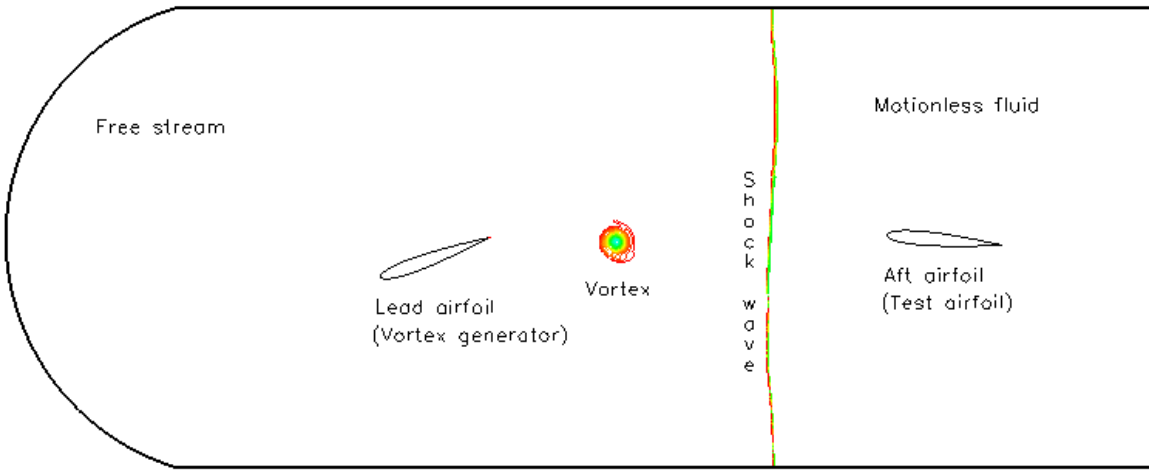

Figure 1: Schematic diagram of the control area, shock wave and vortex illustration.

Numerical Solution and Flow Solver

The numerical domain is divided into nine zones using structured grid topology, as depicted in Figure 2. A parallel processing is performed on three different SGI machines (having two CPU's each) available within the Institute. It is also worth mentioning that the noncontiguous grid (See Figure 3) technique is used to reduce the grid points requirement at distances far away from the vortex path. The Global Newton iteration procedure available in the WIND code [10] is used for time accurate solution. It was found that this technique stabilizes the solution and improves considerably the time accuracy by transferring the entire unsteady convective-diffusive equations on the right-hand side of the matrix solver, and by performing some iterations within each time step over all the defined zones. Therefore, the zone interface boundaries are updated to the new time level, along with the interior flowfield solution. This leads essentially to an implicit treatment of the zone boundaries. The time step is 5×10^{-7} seconds and the number of grid points is roughly one million. The distance of the first node from the viscous walls is chosen such that y+ is varying between 0.5 and 2.5. A large number of grid points are distributed along the vortex path to avoid numerical dissipation. The convergence criterion within each time step is achieved when the maximum local residual of the transport equations is reduced by 3 orders of magnitude.

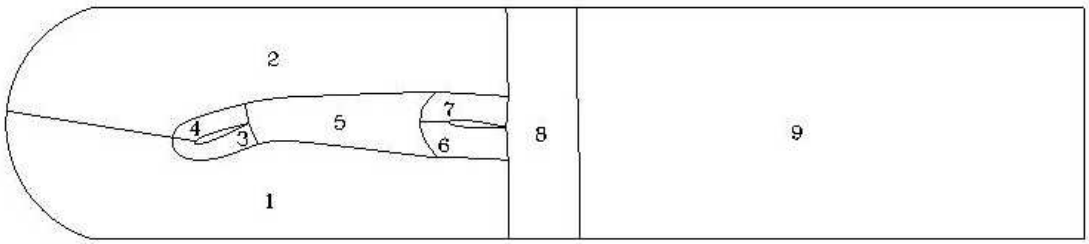

Figure 2: Structured multi-block representation.

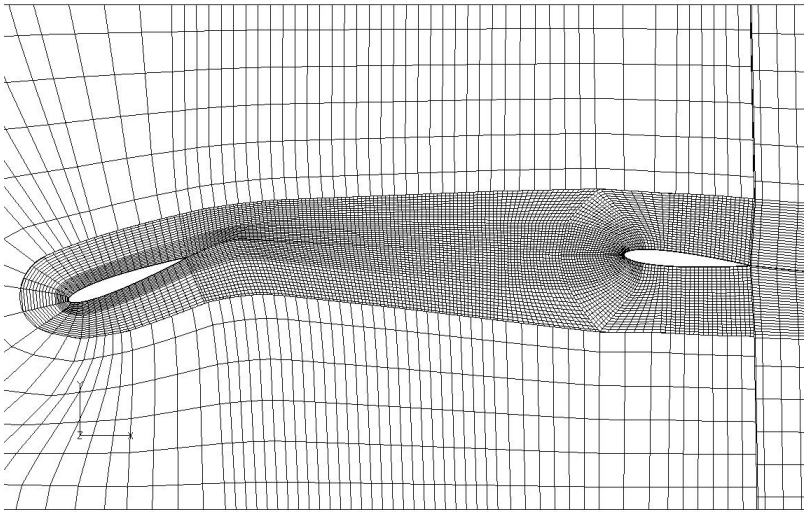

Figure 3: Mesh used for AVI problem. The mesh is coarsened intentionally for clear representation. The actual grid size is ten times smaller than that showed in this figure (closed-up view every 10^{th} line in all zones).

Initial and Boundary Conditions

The freestream conditions implemented for the present computations conformed to those observed experimentally by Sobieraj et al. [3]. As shown in Figure 4, the initial conditions for the flow solver are described by the presence of a shock wave just near the leading edge of the lead airfoil. The shock wave is travelling in a motionless fluid at a Mach number of 1.6. Behind the shock, freestream conditions are assumed to be $M_\infty = 0.69$, $P_\infty = 3.278$ psi, $T_\infty = 731.3^o R$ and $\alpha = 0^o$. Ahead of the shock, stagnation conditions are held at $P_\infty = 1.16$ psi and $T_\infty = 527.4^o R$. Freestream conditions are prescribed at the inlet of the tube. At the outlet, a constant pressure is maintained prior to the arrival of the moving shock. The airfoil surfaces are regarded as viscous boundaries and the tube horizontal walls are described as inviscid boundaries to avoid the vortex-wall boundary layer interaction.

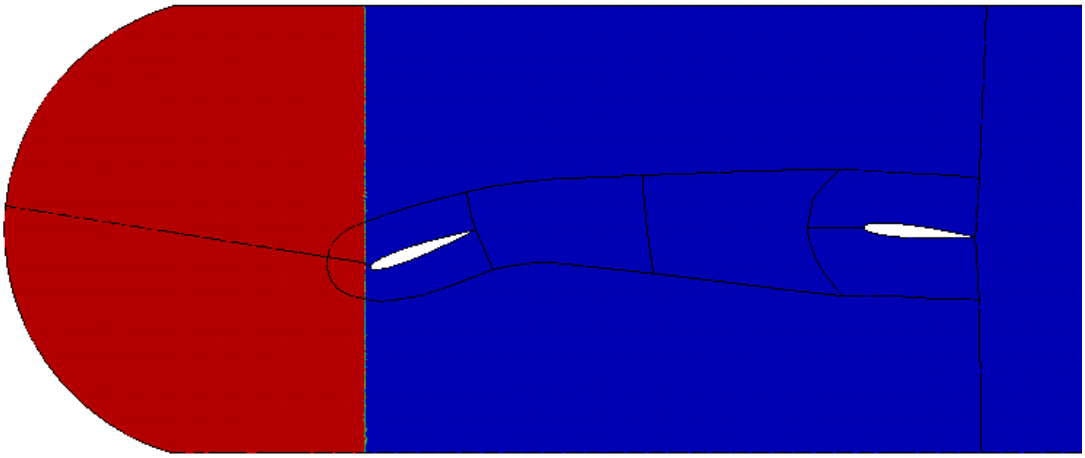

Figure 4: Pressure field for the initial conditions. The left region represents the freestream condition and the right region the motionless fluid. The shock wave is represented by the vertical interface between the two regions.

Results and Discussion

As described in Figure 4, imposing a straight vertical shock wave near the leading edge of the lead airfoil effectively determines the initial conditions for the flow solver. A high-pressure region exists behind the shock wave as it comes close to the lead airfoil, where the flow is assumed to be uniform. Ahead of the shock wave, there exists a low-pressure region where the fluid is motionless and equally undisturbed by any incoming shock waves. Moving forward in time, the shock wave is now travelling at a Mach number of approximately 1.6 and the induced flow behind the shock is at Mach number of 0.69.

In the present work, since the angle of attack of the lead airfoil exceeds the critical angle for stationary stall (-20 degrees nose down), separated and turbulent flows are expected to occur, especially on the lower surface region of the airfoil and along its wake. Thus the flow behavior could be significantly affected by the presence of the viscous effects in the flow. To address the time dependencies present in such flows, the Navier-Stokes equations with appropriate Spalart Allmaras turbulent model equations are solved to describe the flow unsteadiness within the shock tube. The results are presented in terms of the pressure, turbulent viscosity and vorticity contours (or profiles) and the time history of the lift coefficient.

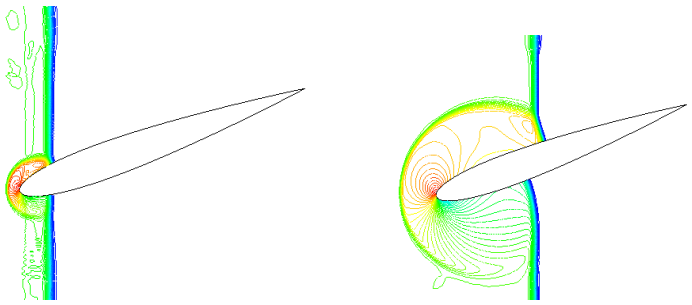

a) t = 0.03 ms. b) t = 0.09 ms.

Figure 5: Pressure distribution behind the shock wave.

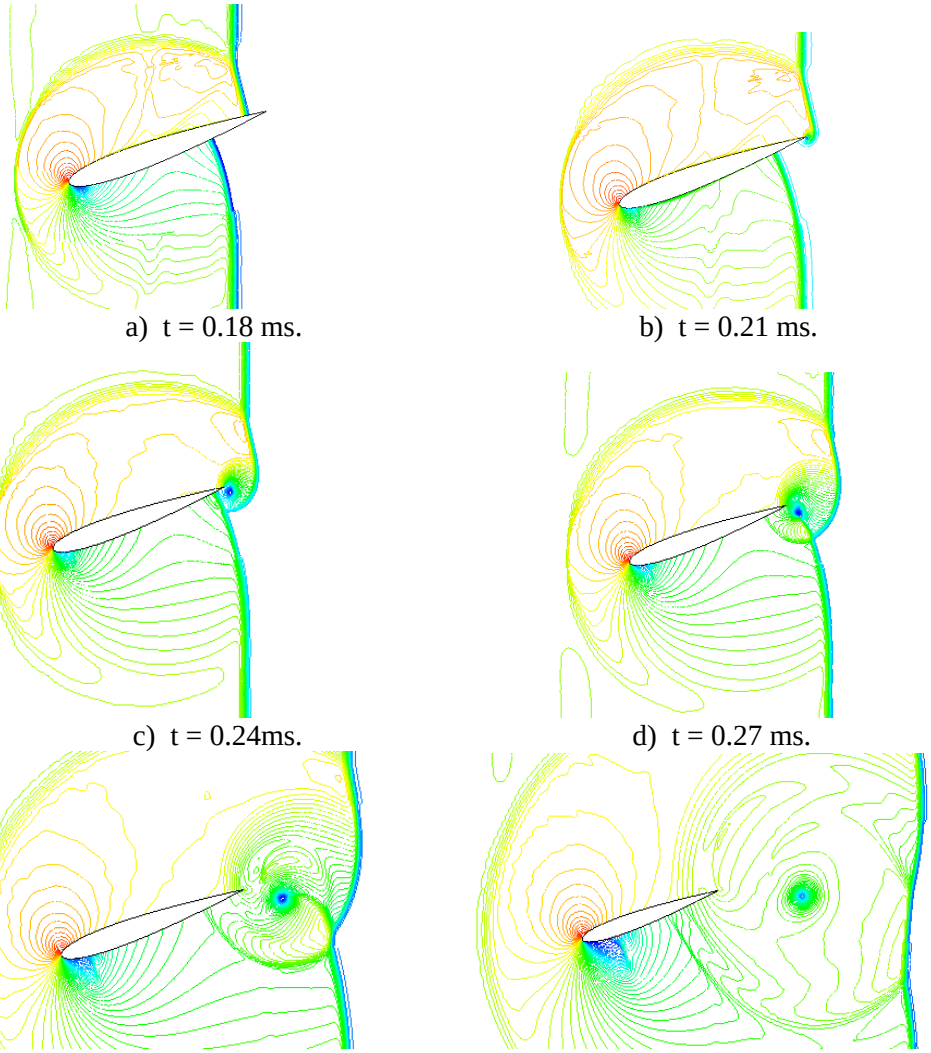

a) t = 0.18 ms. b) t = 0.21 ms.

c) t = 0.24ms. d) t = 0.27 ms.

e) t = 0.33 ms. f) t = 0.51 ms.

Figure 6: Vortex generation process shown in a pressure distribution field.

Airfoil- Shock-Wave Interaction: Generation of a Vortex

As soon as the shock impinges upon the lead airfoil, an airfoil-shock-wave interaction phenomenon begins to occur. After the shock wave has impinged on the airfoil, a reflection compressibility wave is generated which propagates in all directions. Since the impact is strong on the upper surface of the airfoil, as observed in Figure 5, the reflection wave tends to be more enhanced relative to the lower one, in the upper region of the tube. The time sequence of the resulting flowfield as captured in Figure 6 shows that the shock wave is then split into two parts. Owing to the airfoil inclination and the reflected pressure wave, the upper shock wave near the airfoil surface is seen to travel faster than the lower one. As expected, the upper shock arrives first at the trailing edge of the airfoil. The lower one is delayed by about 0.03ms. During this short period, the upper shock travels backward underneath the trailing edge of the airfoil and is virtually responsible for the generation of the start-up vortex. Once the lower shock arrives at the trailing edge, the combined shock system proceeds towards the aft airfoil with the newly created vortex close at its heels. Figure 6 (c–e) show graphically the history of the shock passage followed with the creation and subsequent separation of the vortex at the trailing edge.

As a result of the airfoil-shock-wave interaction, two distinct compressibility waves are generated at the lead airfoil. After 0.51 ms (after impact), as seen in Figure 6 (f), the vortex has drifted a good 1/2 chord length downstream of the lead airfoil at freestream velocity. After 1.05 ms into the flow history, it is observed, as evident from the turbulent viscosity contours in Figure 7, that the flow has begun to separate from underneath the lead airfoil and that turbulence too is present particularly in the inner core of the vortex. Figure 8 displays the flowfield pressure contours at the instant when the moving shock wave is almost midway past the aft airfoil. As for the lead airfoil, a similar reflection compressibility wave is generated when the shock hits the airfoil. The most interesting thing is the vortical flow behavior. As observed in experiment [3], the vortex is nearly symmetric. A downward reflection compressibility wave is also observed right above the vortex. This wave is the reflection from the wall of the original compressibility wave generated during the lead-airfoil-vortex interaction.

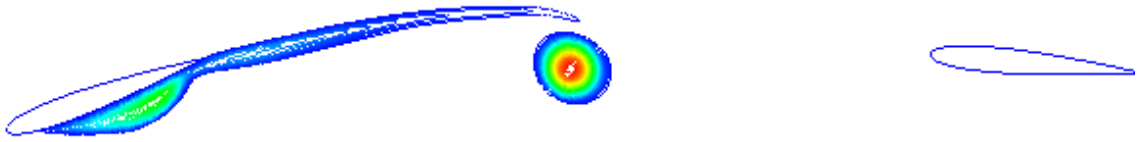

Figure 7: Turbulent viscosity at t = 1.05ms.

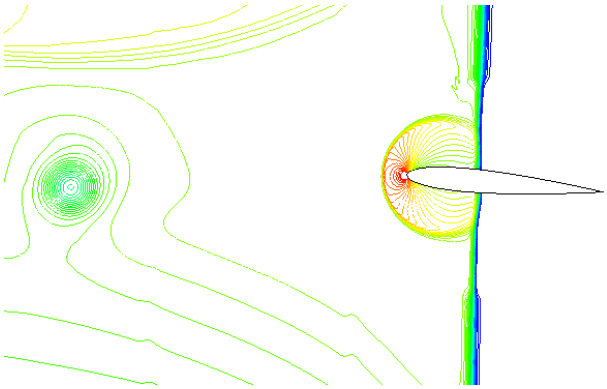

Figure 8: Pressure distribution at t = 1.05 ms when the shock wave passes over the aft airfoil.

A global view of the flow behavior along the shock tube is depicted in Figure 9. At this instant of time, t = 1.35 ms, we can observe a massive flow separation on the lower surface of the lead airfoil. The oblique incident compressibility wave that is reflected from the upper wall is now clearly visible. It is noticed that the pressure wave is disturbed by the presence of the vortex and the aft airfoil. This contributes to the unsteadiness of the flow. Two other circular compressibility waves emanating from the aft airfoil are also clearly visible. The first one was resulted from the shock wave impingement on the leading edge of the airfoil and the second one generated as the shock wave left the trailing edge. The turbulent viscosity and the vorticity contours present in the flowfield are displayed in Figure 10. It was observed that the vortex, when leaving the trailing edge of the lead airfoil, was followed by the lead airfoil wake, which subsequently spreads into a series of small vortices along the wake path (not shown here). This will not affect seriously the AVI process since it remains in the shadow of the stronger well-formed vortex.

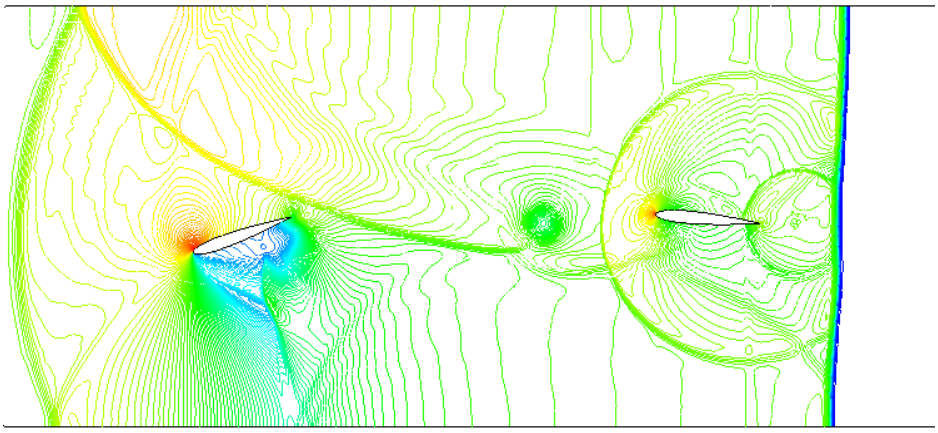

Figure 9: Global view of the pressure distribution within the shock tube at t = 1.35 ms.

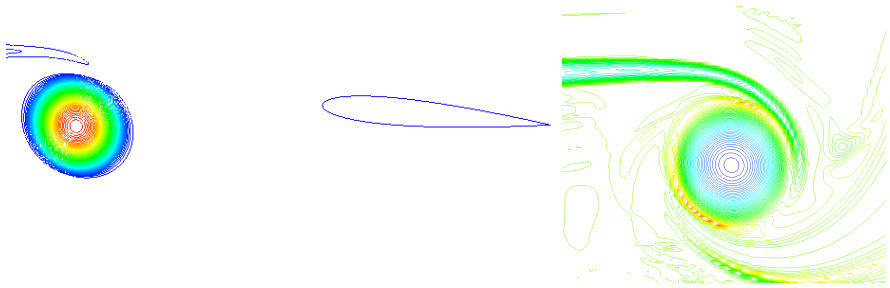

a) b)

Figure 10: Contours of turbulent viscosity a) and vorticity b) at t = 1.35 ms.

Airfoil-Vortex Interaction (AVI)

A close view of the pressure contours around the aft airfoil at different instants of time is shown in Figure 11. The AVI process begins exactly when the vortex appears in the close vicinity of the aft airfoil leading edge. From Figure 11(a), it can be observed that the reflected compressibility wave is seriously affected when the vortex traverses across it. The vortex circulation is clockwise, hence a downwash influence upon the flow is produced near or on the leading edge of the airfoil. As a result, the stagnation point is shifted to the upper surface of the airfoil, which is at an angle

of attack of 5 degrees. Due to the acceleration of the flow below the airfoil, a supersonic flow followed by a shock wave appears below the airfoil leading edge. As the vortex moves forward, as shown in Figure 11(b), the downwash flow becomes more enhanced and the stagnation point is pushed backwards along the upper surface of the airfoil. The compressibility wave, resulting from the passage of the running shock wave at the trailing edge, is seen to move upstream along the airfoil surface. The miss-distance between the vortex core and a horizontal line passing through the leading edge of the airfoil is about -0.14c. When the vortex traverses close to the lower surface of the airfoil, the flow patterns are seen to be notably affected by the passage of the vortex (see for instance Figure 11c and d). For this situation, the low pressure region extends beneath the airfoil due to the flow acceleration caused by the vortex. Hence, a downward lift is generated. The vortex interaction on the airfoil is accompanied by the formation of a compressibility wave near the leading edge which travels upstream of the airfoil. This wave, which is regarded as a source of noise, becomes clearly visible in Figures 11 (e-f).

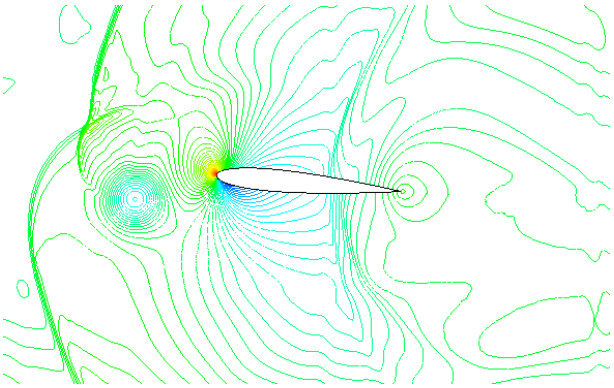

a) t = 1.77 ms.

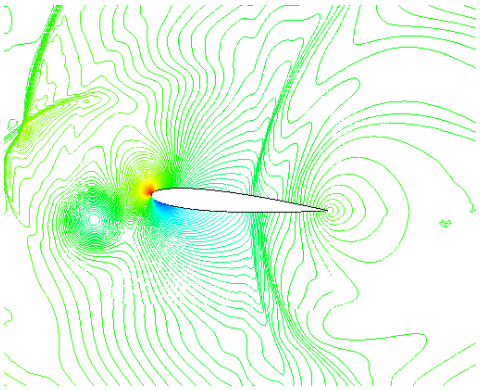

b) t = 1.833 ms.

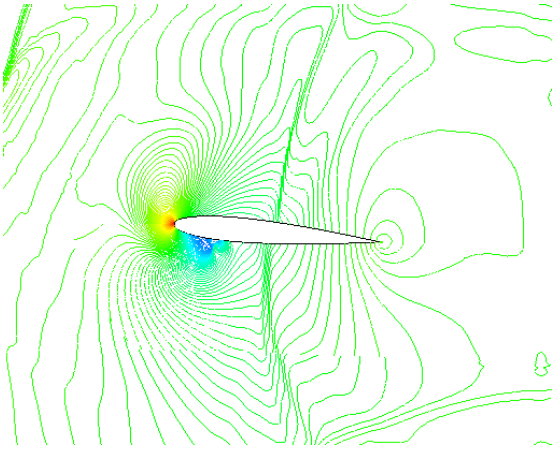

c) t = 2.01 ms.

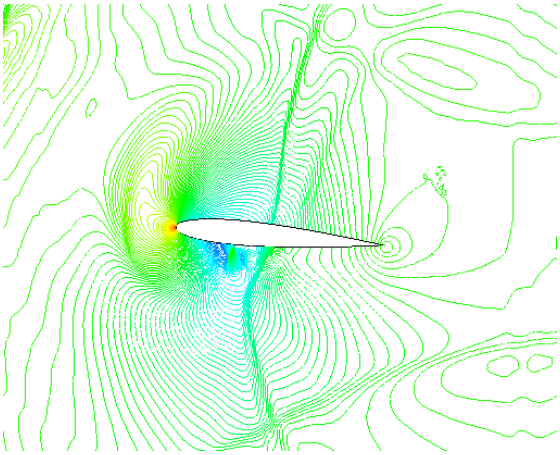

d) t = 2.1 ms.

For captions see next page.

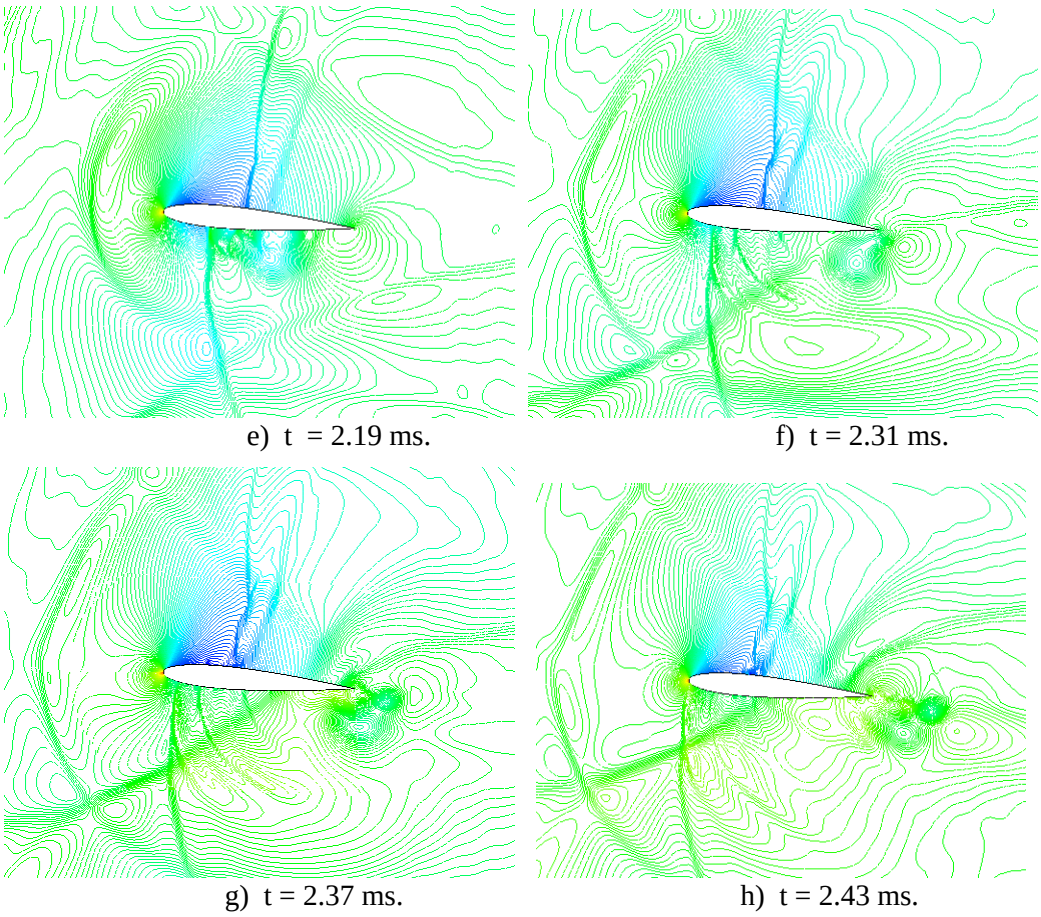

e) t = 2.19 ms. f) t = 2.31 ms.

g) t = 2.37 ms. h) t = 2.43 ms.

Figure 11: Airfoil-Vortex Interaction process: Pressure distribution contours.

When the vortex arrives close to the midway below the airfoil, its effects on the upper surface are weakened as the airfoil physically shields its influence and the flow starts to accelerate (due to finite angle of attack). As a result, the lift is progressively recovered. Furthermore, the dominant shock wave on the upper surface seems to remain stationary, whereas on the lower surface the shock is seen to travel upstream (See Figure 11 e-h). During the AVI process, the vortex strength is reduced but the resulting shear flow in the wake gives rise to a secondary vortex at the trailing edge of the aft airfoil. Two chord downstream, the vortices are seen to be dissipated significantly, mostly from the coarse grid effects.

The time history of the aft airfoil lift coefficient, C_L, is depicted in Figure 12. Experimental results, obtained for a miss-distance of h/c = -0.1, are presented in the same Figure for comparison. The experimental results in the Figure are consistent with a moving shock wave which arrives at the leading edge at t = 1 ms. Since the airfoil is at a given angle of attack, the lift increases progressively as the shock wave moves past the airfoil. The first peak (maximum) on the curve marks the arrival of the reflected compressibility wave from the upper wall, which causes the lift to decrease. When the compressibility wave travels past the aft airfoil, the lift then starts to increase reaching another maximum (second peak) at about t =1.6 ms. At this time, the vortex is in immediate vicinity of the leading edge of the airfoil. As the vortex starts to interact with the airfoil structure, the lift is seen to decrease until t = 2 ms. At this instant, the lift has decreased to a negative (downward force) value of about C_L = -0.5. As the vortex leaves the airfoil, the lift appears to recover dramatically. The reflection compressibility wave from the bottom wall cause the lift to increases more rapidly than the experiment results. During the AVI

process modeled in the current simulations, where the miss-distance was measured to be about -0.14, the time history of the lift, as shown in Figure 12, is seen to agree qualitatively well with the experimental results [3]. The small discrepancy between the present simulations and the experiment results is due probably to reflection compressibility waves from the walls, which are suppressed in the experiment by incorporating triangular slates along the top and the bottom walls of the tube.

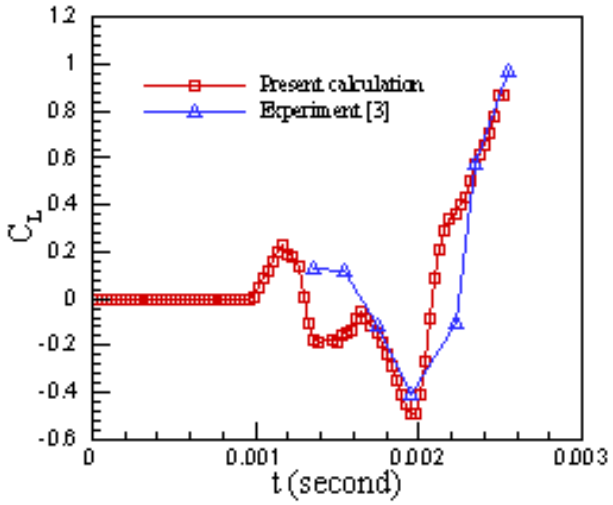

Figure 12: Time history of the lift coefficient C_L for the aft airfoil. Qualitative comparison with experimental data [3].

Conclusion

The present work describes the AVI effects from the numerical simulation of vortex included flow past two NACA 0012 airfoils in tandem contained within a shock tube of rectangular cross section.

The presence of the vortex generated from the lead airfoil has noticeable effects upon the flowfield surrounding the two airfoils. The unsteady flowfield contains highly complex shock wave interaction patterns with airfoils and various other reflecting compressibility waves. The vortex and shock wave interactions are responsible for various noise and vibration issues associated with rotor blade flows. The AVI interaction processes cause various aerodynamic oscillations, including time dependent changes to the aerodynamic loads on the test airfoil.

The two-dimensional based numerical model is a convenient way of studying the fundamental issues related to the noise and vibration aspects of the rotor performance. The expertise developed for two-dimensional unsteady flowfield studies could in turn be extended to more complex 3D simulations.

Acknowledgement

The authors gratefully acknowledge the encouragement and financial support of the Canadian Department of National Defense. The authors are grateful to the NPARC alliance for the use of their WIND code in the present work. The authors are also grateful to Dr. F. François for reviewing this paper.

References

1- Caradonna, F. X., “The Application of CFD to Rotary Wing Flow Problems”, AGARD–R-781, 1990.
2- Piechna, J. and Szumowski, A. P., “Effect of Miss-Distance on the Airfoil-Vortex Interaction: Numerical study”, Arch. Mech., 50, 1, Warazawa, pp. 127-138, 1998.
3- Sobieraj, G., Piechna, J., Selerowicz, W. and Szumowski, A. P., “Effect of Angle of Attack on the Airfoil-Vortex Interaction”, The Arch. Mech. Eng., XLV, 1, pp. 19-30, 1998.
4- Petrini, E., Efraimsson, G. and Nordstrom, J., “A Numerical Study of the Introduction and Propagation of a 2-D Vortex”, The Aeronautical Research Institute of Sweden, FFA TN 1998-66, 1998.
5- Kaminski, W. S. and Szumowski, A. P., “Acoustic Effects of Parallel Vortex-Airfoil Interaction”, Journal of Sound and Vibration, Vol. 183, No 2, pp. 209-220, 1995.
6- Selerowicz, W., Sorbieraj, G. and Szumowski, A. P., “Effect of Miss-Distance on the Airfoil-Vortex Interaction: Experiment”, Arch. Mech., 50, 1, Warazawa, pp. 691-701, 1998.
7- Wittmer, K. S. and Devenport, W. J., “Effects of Perpendicular Blade-Vortex Interaction, Part. 1: Turbulence Structure and Development”, AIAA Journal, Vol. 37, No. 7, pp. 805-812, 1999.
8- Wittmer, K. S. and Devenport, W. J., “Effects of Perpendicular Blade-Vortex Interaction, Part. 2: Parameter Study”, AIAA Journal, Vol. 37, No. 7, pp. 813-817, 1999.
9- Spall, R. E. “Numerical Study of a Wing-Tip Vortex Using the Euler Equations”, Journal of Aircraft, Vol. 38, No. 1, pp. 22-27, 2001.
10- WIND Code manuals, The NPARC Alliance, NASA Glenn Research Center, Cleveland, Ohio, http://www.lerc.nasa.gov/www/wind.

Paper: 12
Author: Dr. Mamou

Question by Dr. Luckring: Interesting calculation, but your flow seems to be irrelevant to helicopter applications due to vortex orientation. For helicopters, the vortex core is roughly perpendicular to the shock; in your calculations it is parallel to the shock.

Answer: Our computations as yet are not directly related to the helicopter flows. This study is more in line with the concept-validating exercise in 2-D. The lead airfoil is used to germinate a vortex, which in turn would interact with the aft airfoil. This type of flow has certain features in common with the blade/vortex problem in rotor flow field studies.

Question 2: Can you simulate the shock tube experiment better?

Answer: We can simulate the shock tube experiment better by solving the problem in 3-D such that the reflection compressibility waves could be cancelled by incorporating triangular states on the top and bottom tube walls.

Question 3: What have you done about computational uncertainty?

Answer: Computational uncertainty was not carried out for the present study. We may investigate this for some of our future work.

Question by Dr. Malmuth: There appears to be a shock being reflected from the wall.

Answer, Dr. Khalid: Is there a question here?

Comment, Dr. Malmuth: I was just making a comment following Dr. Luckring's questions.

Answer, Dr. Khalid: Yes, we came across similar shock reflection during our wall interference work. When you use a reflection boundary condition on the wall, the impinging shock reflects back from the solid wall.

This page has been deliberately left blank

Page intentionnellement blanche